Optimization of chromatic optics in the electron storage ring of the Electron-Ion Collider

Yunhai Cai and Yuri Nosochkov
SLAC National Accelerator Laboratory, 2575 Sand Hill Road, Menlo Park, California 94205, USA

J. Scott Berg, Jorg Kewisch, Yongjun Li, Daniel Marx, Christoph Montag, Steven Tepikian, and Ferdinand Willeke
Brookhaven National Laboratory, Upton, New York 11973, USA

Georg Hoffstaetter and Jonathan Unger
Cornell University, Ithaca, New York 14853, USA

(Received 27 February 2022; accepted 23 June 2022; published 8 July 2022)

We have developed a new chromatic compensation scheme for the electron storage ring with two low-beta interaction regions in the Electron-Ion Collider. The hybrid scheme consists of the modular chromatic matching of periodic systems and beamlines. The first-order chromatically matched solutions are linearly parameterized with the local linear chromaticities that control the higher order chromatic beatings. The parameterization enables an efficient optimization of dynamic aperture. As a result, we successfully achieve the 1% design criterion for the momentum aperture in the ring.

DOI: 10.1103/PhysRevAccelBeams.25.071001

I. INTRODUCTION

To achieve a factory level of luminosity, 10^{34} cm^{-2} s^{-1} in circular colliders, it has been always challenging to focus the colliding beams to an extremely small size at the interaction point (IP) while maintaining an adequate momentum aperture. In the B-factories [1,2], 1% of the off-momentum dynamic aperture was sufficient to accommodate the energy spread of the beam due to synchrotron radiation. For the future e^+e^- colliders [3,4] at much higher beam energy, the required momentum acceptance becomes twice larger for accommodating the beamstrahlung [5]. This requires that the chromatic aberrations generated from the final focusing quadrupoles are locally compensated by the pairs of sextupoles with -I separation in the dedicated module [6,7].

On the other hand, the chromatic compensation in the hadron colliders is carried out by the families of sextupoles in adjacent arcs [8,9], largely because of less chromatic aberrations and smaller momentum aperture required in comparison to the e^+e^- accelerators. Since the Electron-Ion Collider (EIC), as shown in Fig. 1, is a hadron and electron collider, it inherits the characteristics from both the

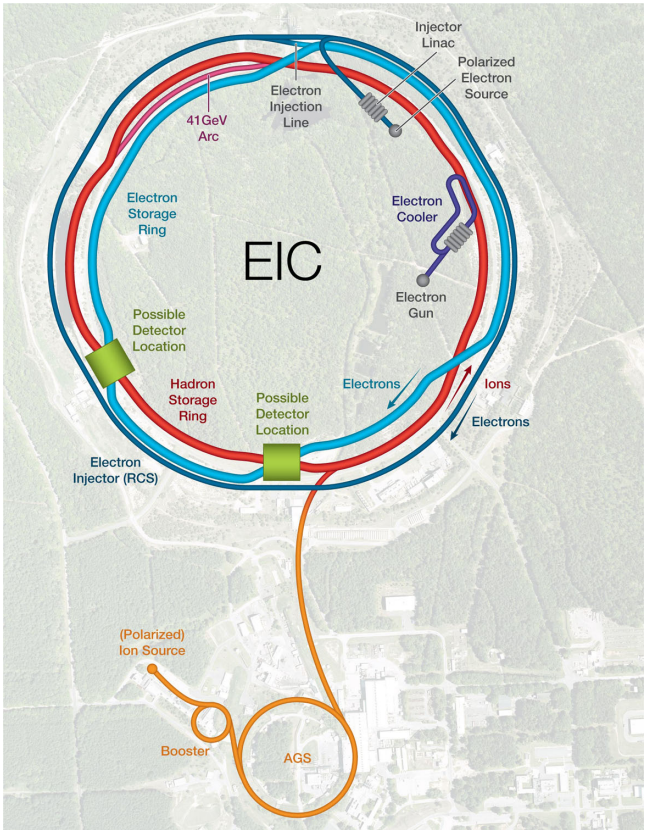

FIG. 1. Schematic layout of the EIC at Brookhaven National Laboratory.

TABLE I. Main parameters of the electron storage ring.

Parameter	Value
Beam energy, E_0 [GeV]	18.0
Circumference, C [m]	3834
Emittance, ϵ_x [nm]	28.4
Energy spread, σ_δ [10^{-4}]	9.6
Damping time, τ_x, τ_y, τ_s [ms]	12.4, 12.5, 6.3
Tune, ν_x, ν_y, ν_s	52.12, 45.10, 0.055
Natural chromaticity, ξ_{0x}, ξ_{0y}	$-106, -110$
IP beta, β_x^*, β_y^* [m]	0.59, 0.057
Distance from IP to quad, L^* [m]	5.3

hadron and the e^+e^- colliders. The challenge to be addressed in this paper is how to achieve the momentum bandwidth of 1% in the new electron storage ring (ESR) with two neighboring low-beta interaction regions (IRs) using the sextupole families in the adjacent arcs.

The EIC will be based on the existing Relativistic Heavy Ion Collider (RHIC) complex, which has a hexagon shape as shown in Fig. 1. As a result, the regions in the ESR, which will be installed in the RHIC tunnel, are named according to a clock: the IRs and straights using even and the arcs odd integers. The ESR will provide polarized electron beams circulating clockwise as indicated in Fig. 1. The electron beam will be brought into collision with polarized protons or light ions, or with unpolarized heavy ions, stored in the existing hadron storage ring. The design of the ESR with one low-beta IR (IR6 centered at a 6-hour position) based on the semilocal chromatic compensation scheme was successfully completed [10]. Including a second low-beta IR (IR8 centered at an 8-hour position) remains a challenge [11] because of the extra chromaticity.

The required center-of-mass energy range of the EIC from 29 to 140 GeV will be realized by proton energies that range from 41 to 275 GeV and by electron energies that range from 5 to 18 GeV. The main design parameters relevant to the performance of single-particle dynamics are tabulated in Table I. The 18-GeV energy is chosen for this study because of its largest value of the rms energy spread, approaching 0.1%. This leads to an absolutely minimum required momentum aperture of 0.6% to ensure an adequate quantum lifetime for the electron beam. Along with the largest chromaticity of two IRs, this set of parameters presents the most difficult case for the chromatic compensation and dynamic aperture.

The betatron tunes are selected by the optimization of the spin dynamics as well as the beam-beam interaction. They are very close to integers, making the chromatic compensation even more difficult. In this study, they are fixed to the values in the table.

II. LATTICE

It is always challenging to design a final focusing system in a circular collider. In the EIC, it becomes even more so because of a small β_y^* and a very large L^*, resulting in the high beta peaks shown in Fig. 2 and large natural chromaticity in Table I.

Moreover, because of the polarization requirement, spin rotators are necessary between the arcs and the low-beta IRs to rotate the polarization from the vertical direction in the arcs to the longitudinal direction at the IP. As a result, a local chromatic compensation with -I paired noninterlaced sextupoles cannot be deployed due to a lack of space for dedicated sextupole optics in the IR. Therefore the correction has to be carried out by the sextupoles far away in the arcs. Finally, the crossing angle, crab cavities, spectrometer dipole, and the need of mitigating the synchrotron radiation into the detector make the IR more complicated and even asymmetric as shown in Fig. 2.

A 90° phase advance of regular FODO cells in the arcs is chosen to obtain the required emittance at 18 GeV to match the horizontal beam sizes in the collision. We place two

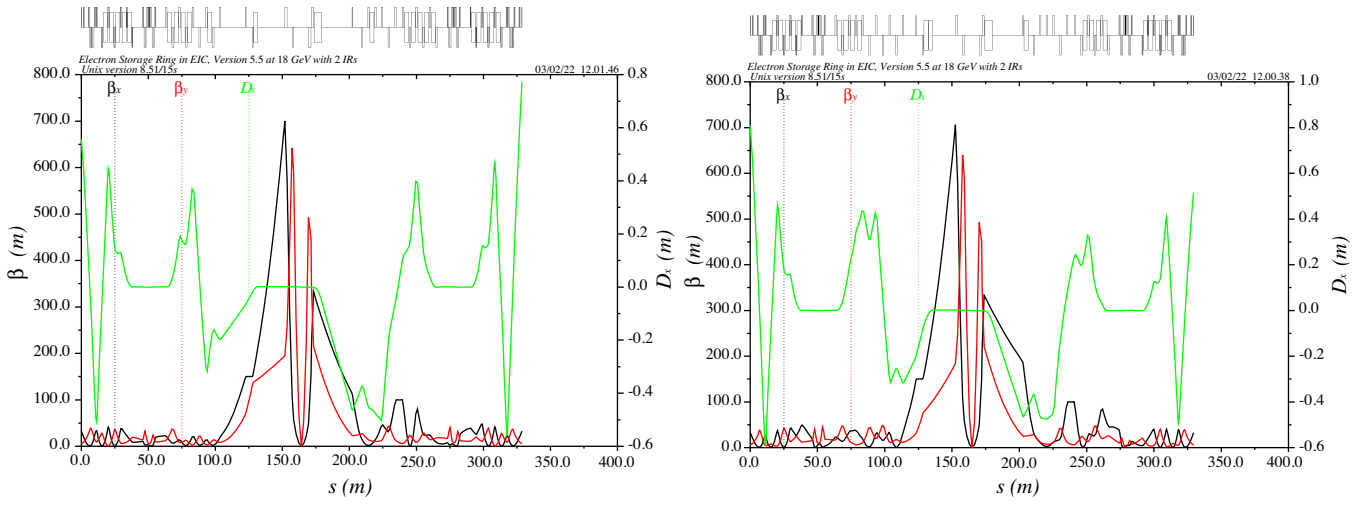

FIG. 2. Lattice functions in the interaction region 6 (left) and 8 (right).

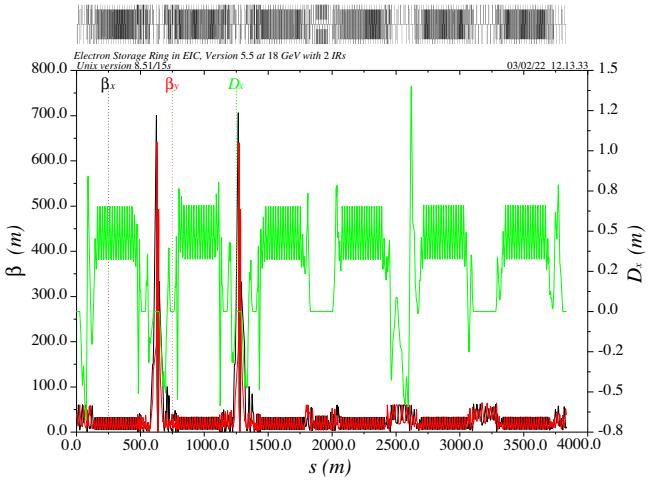

FIG. 3. Lattice functions in the electron storage ring with two interaction points starting from the center of straight-4.

families of sextupoles in 16 regular cells of each arc to compensate for the linear chromaticity. Since every four cells make a unit transformation of betatron oscillation, the third-order driving terms within one betatron unit are all canceled out [12]. The ring consists of six arcs and six straight sections as depicted in Fig. 1. The full lattice including two low-beta IRs is shown in Fig. 3.

To characterize the nonlinear property of the lattice, we compute the tune shifts along with the high-order chromaticities using the normal form analysis [13,14] and tabulate the result in Table II. The linear chromaticity is set to one unit in both planes using two families of sextupoles. The second-order chromaticities are reasonably small values because the phase advances between the two IPs are set at $11.25 \times 2\pi$ and $7.25 \times 2\pi$ in the horizontal and the vertical planes, respectively, to cancel the large

TABLE II. Normal form analysis in the ring with two global families of sextupoles.

Derivatives of tunes	Value
$\partial\nu_{x,y}/\partial\delta$	1, 1
$\frac{1}{2!}\partial^2\nu_{x,y}/\partial\delta^2$	$-204, \ -15$
$\frac{1}{3!}\partial^3\nu_{x,y}/\partial\delta^3$	$-8.36 \times 10^4, \ -3.02 \times 10^5$
$\frac{1}{4!}\partial^4\nu_{x,y}/\partial\delta^4$	$-5.17 \times 10^6, \ -1.23 \times 10^8$
$\partial\nu_x/\partial J_x \ [m^{-1}]$	2.91×10^3
$\partial\nu_x/\partial J_y \ [m^{-1}]$	-1.52×10^4
$\partial\nu_y/\partial J_y \ [m^{-1}]$	9.74×10^3

first-order chromatic beta beatings from the IR final focus quadrupoles. Based on our experience, the values of the tune shift vs amplitude seem sufficiently small, but the high-order chromaticities are far too large to achieve 1% momentum aperture. These very high values are confirmed by the numerical computation presented in the right plot of Fig. 4, where chromaticity walls are seen at $\pm 0.4\%$ in the vertical plane. How to reduce the nonlinear chromaticity and eliminate the walls are the challenges addressed in this paper.

We evaluate the dynamic aperture of the ESR by tracking the particles with various momenta. The tracking is carried out with both synchrotron oscillations and radiation damping. The left plot of Fig. 4 shows the dynamic aperture in terms of beam sigmas. The horizontal emittance is quoted in Table I, whereas the vertical emittance has been set as half of the horizontal one in the assumption of full coupling. The degradation of the off-momentum aperture is so large that there is not sufficient momentum acceptance to retain the particles in the energy distribution expected from synchrotron radiation. It is clear that we have to make proper chromatic compensation for the IRs in order to increase the momentum aperture of the ESR.

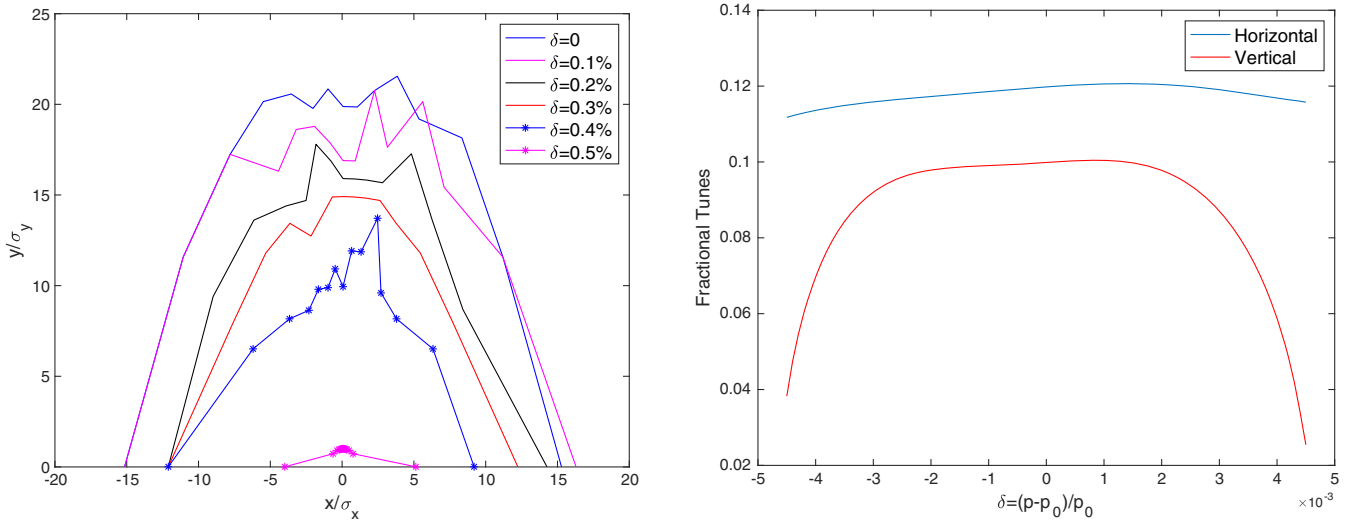

FIG. 4. Dynamic aperture (left) and chromatic tune (right) in the lattice with two global families of sextupoles.

III. PERTURBATION THEORY

We start with the well-known transport matrix from position 1 to position 2,

$$M_{12} = \begin{pmatrix} \sqrt{\frac{\beta_2}{\beta_1}}(\cos\psi_{12} + \alpha_1 \sin\psi_{12}) & \sqrt{\beta_1\beta_2}\,\sin\psi_{12} \\ -\frac{1}{\sqrt{\beta_1\beta_2}}[(1+\alpha_1\alpha_2)\sin\psi_{12} + (\alpha_2-\alpha_1)\cos\psi_{12}] & \sqrt{\frac{\beta_1}{\beta_2}}(\cos\psi_{12} - \alpha_2\,\sin\psi_{12}) \end{pmatrix}, \tag{1}$$

where $\beta_{1,2}$ and $\alpha_{1,2}$ are the Courant-Snyder parameters at the positions 1 and 2, respectively and ψ_{12} is the phase advance between them. Given the lattice parameters at a position s_1 in the ring, we may define an "ascript" matrix A as

$$A = \begin{pmatrix} \sqrt{\beta_1} & 0 \\ -\frac{\alpha_1}{\sqrt{\beta_1}} & \frac{1}{\sqrt{\beta_1}} \end{pmatrix}. \tag{2}$$

Denoting with M_{12}, the transport matrix from s_1 to any other point s_2, it is easy to verify that the Twiss parameters in s_2 are given by

$$\begin{aligned} \beta &= B_{11}^2 + B_{12}^2, \\ \alpha &= -(B_{11}B_{21} + B_{12}B_{22}), \\ \psi &= \tan^{-1}(B_{12}/B_{11}). \end{aligned} \tag{3}$$

with B defined as

$$B = M_{12}A. \tag{4}$$

Now we consider a small quadrupole error represented by a matrix,

$$M_q = \begin{pmatrix} 1 & 0 \\ -q & 1 \end{pmatrix}, \tag{5}$$

at the position 2 and calculate the perturbed lattice functions at the position 3 down the beamline. The transport matrix is $M = M_{23} \cdot M_q \cdot M_{12}$, where M_{23} is the transport matrix from the position 2 to 3 which of course has the same form as in Eq. (1) with replaced indices. Then the perturbed matrix B is given by $B = M \cdot A$ and using Eq. (3), we have the perturbed lattice functions at the first order of q,

$$\beta = \beta_3 - q\beta_2\beta_3\,\sin 2\psi_{23}, \tag{6}$$

$$\alpha = \alpha_3 + q\beta_2(\cos 2\psi_{23} - \alpha_3\,\sin 2\psi_{23}), \tag{7}$$

$$\psi = \psi_{13} + q\beta_2(1 - \cos 2\psi_{23})/2. \tag{8}$$

We see that the beating wave propagates at twice the betatron phase from the source of the error down to the observation position even in the phase advance itself. Focusing on the perturbed parts in Eqs. (6) and (7) and introducing the functions, $a = \Delta\alpha - \alpha_3\Delta\beta/\beta_3$ and $b = \Delta\beta/\beta_3$, we obtain,

$$a = q\beta_2\,\cos 2\psi_{23}, \tag{9}$$

$$b = -q\beta_2\,\sin 2\psi_{23}, \tag{10}$$

which simply propagate orthogonally at the twice of the betatron phase. With multiple quadrupoles, we simply sum all individual contributions as the first-order perturbation,

$$a = \sum_i q_i\beta_i\,\cos 2\psi_i, \tag{11}$$

$$b = -\sum_i q_i\beta_i\,\sin 2\psi_i, \tag{12}$$

where ψ_i is the phase advance from the source position "i" to the end of the beamline. For the first-order chromatic perturbation due to quadrupoles, it is $q = -\delta K_1 L_Q$, where $\delta = (p - p_0)/p_0$ is the momentum deviation, K_1 and L_Q are the strength and length of the quadrupole, respectively. Focusing strength of a sextupole due to δ is $q = \delta\eta_x K_2 L_S$, where η_x is the horizontal dispersion and K_2 and L_S are the strength and length of the sextupole, respectively. In general, we need to consider the chromatic beatings in both horizontal and vertical planes. Assuming our previous analysis is for the horizontal plane, then the result in the vertical plane can be obtained by a substitution of $q \to -q$, $\beta_x \to \beta_y$, and $\psi_x \to \psi_y$. $a_{x,y}$ are related to the Montague functions $A_{x,y}$ [15] by $A_{x,y} = a'_{x,y}$ and $B_{x,y} = b'_{x,y}$, where the prime represents the derivative with respect to δ. From Eqs. (11) and (12), their expression at the end of the beamline, s_0, is given by

$$\begin{aligned} A_{x,y}(s_o) = \mp \int_0^{s_o} &[K_1(s) - \eta_x(s)K_2(s)]\beta_{x,y}(s) \\ &\times \cos 2[\psi_{x,y}(s_o) - \psi_{x,y}(s)]ds, \end{aligned} \tag{13}$$

$$\begin{aligned} B_{x,y}(s_o) = \pm \int_0^{s_o} &[K_1(s) - \eta_x(s)K_2(s)]\beta_{x,y}(s) \\ &\times \sin 2[\psi_{x,y}(s_o) - \psi_{x,y}(s)]ds, \end{aligned} \tag{14}$$

where $s = 0$ is the beginning of the considered beamline, in our case the IP. Integrals are used instead of sums because

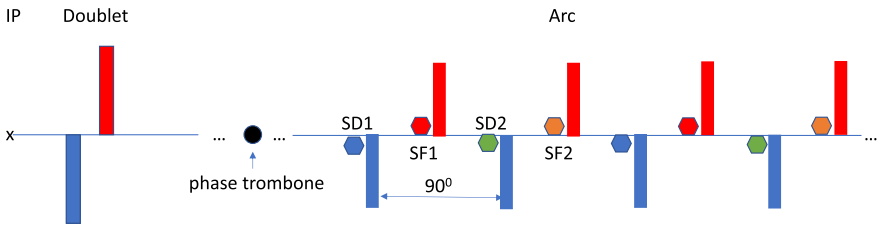

FIG. 5. Scheme of chromatic compensation on one side of low-beta IR using the four sextupole families in the adjacent arc where the vertical bars are quadrupoles and the hexagons are sextupoles.

the quadrupoles near the IP can be very strong often with large variation of beta functions inside. The amplitude of the Montague functions, $W_{x,y} = \sqrt{A_{x,y}^2 + B_{x,y}^2}$, is known as the W function.

Since the IR is a part of beamline in the collider ring, we need to not only correct the chromatic beta beating, as we have shown, but also its linear chromaticity, $\xi_{x,y} = \psi'_{x,y}/2\pi$. Using Eq. (8), we similarly derive the integrals,

$$\xi_{x,y} = \mp\frac{1}{4\pi}\int_0^{s_o}[K_1(s) - \eta_x(s)K_2(s)]\beta_{x,y}(s)ds - \frac{1}{4\pi}A_{x,y}(s_0), \tag{15}$$

where the term $A_{x,y}(s_0)$ is given by Eq. (13).

IV. SEMILOCAL CHROMATIC COMPENSATION

As one can see from Eqs. (13) and (14), the beta beating propagates at twice the betatron phase, therefore the conventional two families of sextupoles (one per plane) in the 16 regular cells do not generate any beating because of 90° phase advance per cell. So we split the two families into four families as illustrated in Fig. 5. This pattern of the sextupoles for the optics with 90° cells was investigated [16] for the HERA (Hadron–Elektron Ring Anlage) design but not used. However, HERA feathered a similar pattern with three families of sextupoles per plane in 60° cells for compensating linear chromaticity and beta-beating.

The difference in strengths of the two sextupoles in two adjacent cells generates beating which adds up linearly in the arc. However, the generated beating from the sextupoles is in the same phase due to the 90° cells. Therefore, it is necessary to introduce a phase trombone that aligns the beating with the chromatic aberration in the IR. On the other hand, two sextupoles of equal strengths 90° apart do not contribute to the beatings but add up to the linear chromaticity.

A. Beta beating

Considering one side of the IR and the adjacent arc shown in Fig. 5, we can find the difference strengths $\Delta S_F = K_2^{(F1)} - K_2^{(F2)}$ and $\Delta S_D = K_2^{(D1)} - K_2^{(D2)}$ and the two phase shifts $\Delta\psi_x$ and $\Delta\psi_y$ introduced by the trombone using Eqs. (13) and (14). Let us start with the Montague functions created by quadrupoles with the trombone (see Fig. 5) which can be written as,

$$A_{x,y} = A_{x,y}^{(<)}\cos 2\Delta\psi_{x,y} + B_{x,y}^{(<)}\sin 2\Delta\psi_{x,y} + A_{x,y}^{(>)}, \tag{16}$$

$$B_{x,y} = B_{x,y}^{(<)}\cos 2\Delta\psi_{x,y} - A_{x,y}^{(<)}\sin 2\Delta\psi_{x,y} + B_{x,y}^{(>)}, \tag{17}$$

where,

$$A_{x,y}^{(<)} = \mp\int_0^{s_t} K_1(s)\beta_{x,y}(s)\cos 2[\psi_{x,y}(s_o) - \psi_{x,y}(s)]ds, \tag{18}$$

$$B_{x,y}^{(<)} = \pm\int_0^{s_t} K_1(s)\beta_{x,y}(s)\sin 2[\psi_{x,y}(s_o) - \psi_{x,y}(s)]ds, \tag{19}$$

where s_t is the position of the trombone and the superscript "<" indicates the integration region before the trombone and

$$A_{x,y}^{(>)} = \mp\int_{s_t}^{s_o} K_1(s)\beta_{x,y}(s)\cos 2[\psi_{x,y}(s_o) - \psi_{x,y}(s)]ds, \tag{20}$$

$$B_{x,y}^{(>)} = \pm\int_{s_t}^{s_o} K_1(s)\beta_{x,y}(s)\sin 2[\psi_{x,y}(s_o) - \psi_{x,y}(s)]ds, \tag{21}$$

are the integrals in the region after the trombone. Since the final focusing quadrupoles are the largest sources of the chromatic beta beatings, it is $A_{x,y}^{(<)}(B_{x,y}^{(<)})$ larger than $A_{x,y}^{(>)}(B_{x,y}^{(>)})$. Note that $\psi_{x,y}$ are the phase advances without the trombone. The strengths of the sextupoles required to cancel the quadrupole beta beatings can be obtained by solving two linear equations in the horizontal plane and are given by

$$\Delta S_F = -\frac{1}{N_S L_S \beta_F \eta_F}(A_x\cos 2\psi_F - B_x\sin 2\psi_F), \tag{22}$$

$$\Delta S_D = \frac{1}{N_S L_S \beta_D \eta_D}(B_x \cos 2\psi_F + A_x \sin 2\psi_F), \quad (23)$$

where N_S is the number of sextupoles per family, $\beta_{F,D}$ and $\eta_{F,D}$ are the horizontal beta and dispersion functions at the position F or D, and ψ_F is the horizontal phase advance from the first "F" sextupole to the end of the beamline.

Similarly in the vertical plane, we have,

$$\Delta S_F = \frac{1}{N_S L_S \beta_D \eta_F}(A_y \cos 2\psi_F - B_y \sin 2\psi_F), \quad (24)$$

$$\Delta S_D = -\frac{1}{N_S L_S \beta_F \eta_D}(B_y \cos 2\psi_F + A_y \sin 2\psi_F). \quad (25)$$

Here we have used the relations of the horizontal and vertical lattice functions in the 90° FODO cells to simplify the expressions. In order to have an univocal solution, the right-hand side of Eqs. (22) and (24) and of Eqs. (23) and (25) must be equal, that is

$$\frac{1}{\beta_F}(A_x \cos 2\psi_F - B_x \sin 2\psi_F) + \frac{1}{\beta_D}(A_y \cos 2\psi_F - B_y \sin 2\psi_F) = 0, \quad (26)$$

$$\frac{1}{\beta_D}(B_x \cos 2\psi_F + A_x \sin 2\psi_F) + \frac{1}{\beta_F}(B_y \cos 2\psi_F + A_y \sin 2\psi_F) = 0. \quad (27)$$

These two coupled equations can be used to find the phase shifts $\Delta\psi_x$ and $\Delta\psi_y$ of the trombone. Analytic solutions are not known in general. But their numerical solutions can be searched easily. Multiple solutions should be expected because of the trigonometric functions involved.

Once the phase shifts are found, the difference in strengths of the sextupoles, $\Delta S_F = K_2^{(F1)} - K_2^{(F2)}$ and $\Delta S_D = K_2^{(D1)} - K_2^{(D2)}$, can be obtained using Eqs. (22) and (23) or Eqs. (24) and (25). It is worth noting that these differences can be implemented by changing beta functions at the sextupoles using a dedicated on-momentum beta beating along the arc [8]. However, these beta beatings may reduce the dynamic aperture due to the high-order multipole errors in the dipole in proton storage rings or increase the emittance in electron rings.

B. Chromaticity

Since the IR is a part of the beamline in the collider ring, we need to not only correct the chromatic beta beating as we have shown but also the linear chromaticity. Here, we consider the beamline where the Montague functions have been corrected as described in the previous section. Equation (15) for the linear chromaticity can be simplified to

$$\xi_{x,y} = \mp\frac{1}{4\pi}\int_0^{s_o}[K_1(s) - \eta_x(s)K_2(s)]\beta_{x,y}(s)ds. \quad (28)$$

It can be seen that only the sum of the strengths $\Sigma S_F = K_2^{(F1)} + K_2^{(F2)}$ and $\Sigma S_D = K_2^{(D1)} + K_2^{(D2)}$ contribute to linear chromaticity. They can be derived by solving two linearly coupled equations. The result is given by

$$\Sigma S_F = \frac{4\pi}{N_s L_S \eta_F(\beta_F^2 - \beta_D^2)}[\beta_F(\xi_x - \xi_x^{(0)}) + \beta_D(\xi_y - \xi_y^{(0)})], \quad (29)$$

$$\Sigma S_D = -\frac{4\pi}{N_s L_S \eta_D(\beta_F^2 - \beta_D^2)}[\beta_D(\xi_x - \xi_x^{(0)}) + \beta_F(\xi_y - \xi_y^{(0)})], \quad (30)$$

where $\xi_{x,y}^{(0)}$ is the natural chromaticity,

$$\xi_{x,y}^{(0)} = \mp\frac{1}{4\pi}\int_0^{s_o} K_1(s)\beta_{x,y}(s)ds. \quad (31)$$

Given the chromaticity $\xi_{x,y}$, the strengths of the four families of sextupoles are completely determined. Combining the difference solution in Eq. (22) or Eq. (24) with the sum solution in Eq. (29), we obtain the settings of the two families of F sextupoles, and correspondingly, for the two D families. It is easy to show that the settings can be linearly parameterized by the two continuous values of linear chromaticity for a given phase trombone. The parameterization enables an efficient optimization of the dynamic aperture.

C. Numerical solution

Meanwhile, we also use the previously developed code [17] that is capable of computing an arbitrary order of derivatives of the lattice functions with respect to the momentum. Using the downhill simplex optimizer [18], we find directly the settings of the four families of the sextupoles along with two-phase shifts of the trombone. The six equally weighted goals are four Montague functions $A_{x,y} = B_{x,y} = 0$ and the linear chromaticity ξ_x and ξ_y at selected values at the end of the beamline. For a simplified interaction region without solenoid, we find excellent agreement between the perturbation theory and the numerical method for the case with no initial chromatic beatings at the beginning of the beamline.

We first consider the region from the beginning of the lattice (center of straight-4) to the first interaction point (IP6) in Fig. 3. The optimal solution obtained by the numerical search is shown in the left plot of Fig. 6 in terms of $W_{x,y}$. The W functions are nearly zero at the IP6 and rise to the peak at the final focusing quadrupoles. Then they are

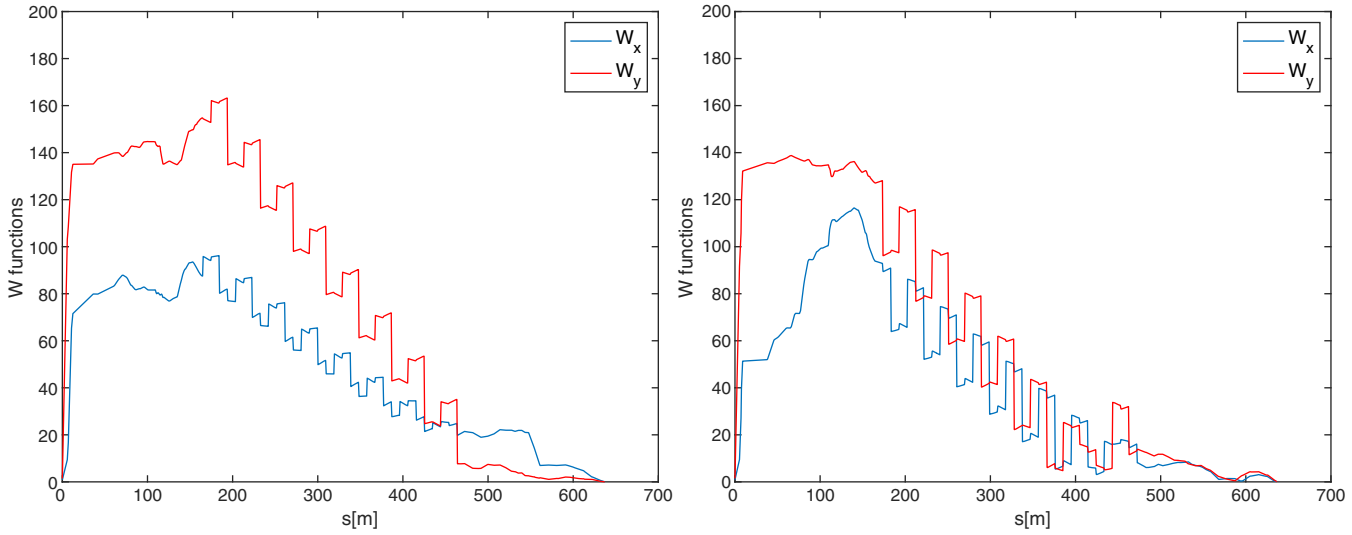

FIG. 6. Amplitudes of the W functions in the upstream of the IR6 (left) and the downstream of the IR8 (right) using four families of sextupoles in the adjacent arcs, where IP is at $s = 0$.

linearly reduced by the sextupoles in the adjacent arc, finally reaching zero at the center of the straight 4. The periodically reducing peaks along the arc correspond to the eight periods of the sextupole scheme. Note that the direction of the beamline in Fig. 6 (left) is opposite compared to Fig. 3. The initial condition is obtained by enforcing a periodic solution between the IP6 and IP8 and tabulated in the third column of Table III. Since the matching beamline goes backward, the signs of $\alpha_{x,y}(\delta)$ are flipped. The linear chromaticity is set at -6 and -2 in the horizontal and the vertical planes, respectively. The values are optimized in the tracking for maximum dynamic aperture in the ring. It is worth noting that the vertical phase difference between the final focusing quadrupole and the strongest D sextupole family is $2.5 \times 2\pi$, which differs from a multiple of 2π in the achromatic telescopic squeezing (ATS) scheme [8]. Similarly, we match the first-order chromatic optics from the IP8 to the center of the straight 10, where the rf cavities are placed. There is no need to switch the signs of $\alpha_{x,y}(\delta)$ since the matching beamline is not reversed. The W functions are depicted in the right plot of Fig. 6. The best linear chromaticity is 3.5 and 7 in the horizontal and the vertical planes, respectively. Interestingly, in this case, the vertical phase difference between the final focusing quadrupole and the strongest D sextupole family is $2 \times 2\pi$, as is expected from the ATS scheme.

D. Chromatic mismatch parameter

To consider the higher order chromatic beta beatings, we begin with the well-known mismatch parameter [19],

$$B_{mag}(\delta) = \frac{1}{2}[\gamma(0)\beta(\delta) - 2\alpha(0)\alpha(\delta) + \beta(0)\gamma(\delta)], \quad (32)$$

where $\gamma(\delta) = [1 + \alpha(\delta)^2)]/\beta(\delta)$. This parameter is often used to measure the mismatch between the linear optics and the beam ellipse [20]. Here we use it to measure the mismatch between the design (on-momentum) and the chromatic optics (off-momentum) optics. Expanding α, β, γ to the first order and B_{mag} to the second order of δ, we find,

$$B_{mag} \approx 1 + \frac{1}{2}W^2\delta^2, \quad (33)$$

where W is the Montague function we have introduced previously. This relationship between Sands B_{mag} and

TABLE III. The nonlinear chromaticities and chromatic beatings at the IPs.

Minimized parameters	Two families	Eight families
$\partial\nu_{x,y}/\partial\delta$	$-14.57, -16.89$	$-12.72, -10.48$
$\frac{1}{2!}\partial^2\nu_{x,y}/\partial\delta^2$	$-6.37 \times 10^4, -6.35 \times 10^4$	$-9.60 \times 10, -1.52 \times 10^2$
$\frac{1}{3!}\partial^3\nu_{x,y}/\partial\delta^3$	$-2.02 \times 10^{11}, -2.02 \times 10^{11}$	$2.45 \times 10^4, 3.46 \times 10^3$
$W_{x,y}$	8.56, 5.90	0.91, 1.44
$W^{(2)}_{x,y}$	$1.73 \times 10^5, 1.69 \times 10^5$	38.70, 34.39
$W^{(3)}_{x,y}$	$5.53 \times 10^{11}, 5.59 \times 10^{11}$	$3.09 \times 10^4, 2.25 \times 10^4$

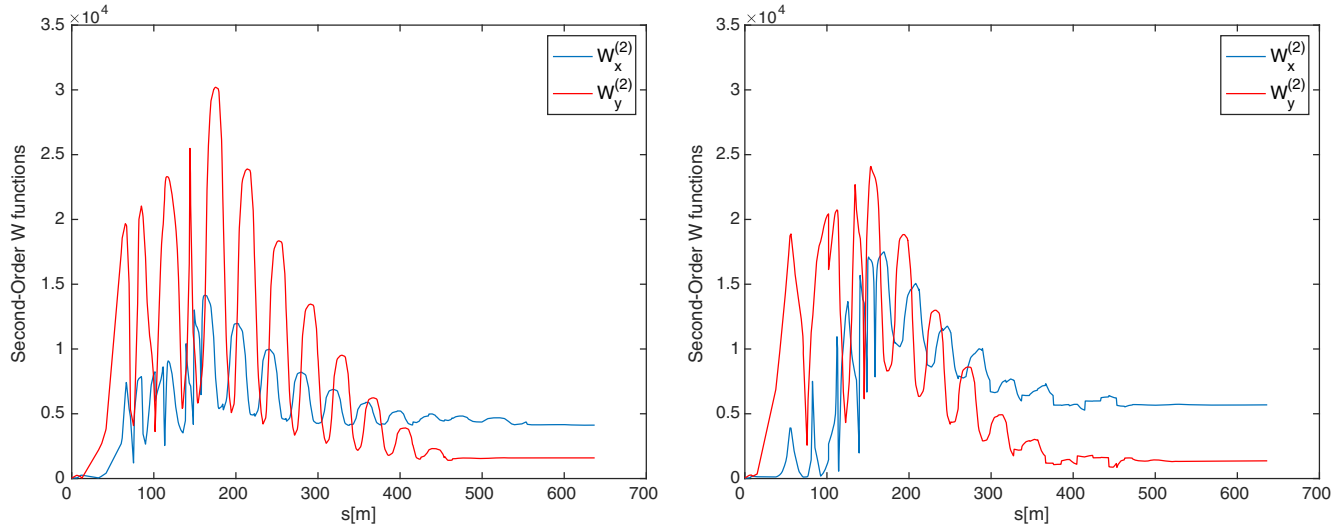

FIG. 7. Amplitudes of the second-order Montague functions in the upstream of the IR6 (left) and the downstream of the IR8 (right) using four families of sextupoles in the adjacent arcs.

Montague W should not be too surprising since both are concerned about the invariance of the mismatch. To extend the expression to higher orders, let us define the nth-order Montague functions as,

$$A^{(n)} = \frac{1}{n!}\left[\frac{\partial^n \alpha(\delta)}{\partial \delta^n} - \frac{\alpha(0)}{\beta(0)}\frac{\partial^n \beta(\delta)}{\partial \delta^n}\right], \tag{34}$$

$$B^{(n)} = \frac{1}{n!}\frac{1}{\beta(0)}\frac{\partial^n \beta(\delta)}{\partial \delta^n}, \tag{35}$$

where $n!$ is introduced to be consistent to the coefficients of the Taylor expansion. In general, the high order of expansion of B_{mag} is too complicated to be useful. For the purpose of chromatic compensation, we assume that all the lower order of Montague functions have been perfectly corrected, namely $A^{(i)} = B^{(i)} = 0$ for $i < n$. As a result, we obtain a similar expression,

$$B_{mag} \approx 1 + \frac{1}{2} W^{(n)2} \delta^{2n}, \tag{36}$$

where $W^{(n)}$ is the amplitude of the n^{th}-order Montague functions, $W^{(n)} = \sqrt{A^{(n)2} + B^{(n)2}}$.

Clearly, the high-order W functions precisely quantify the residual of the chromatic perturbation. Our best first-order solution of matching the chromatic beta beatings also dramatically reduces the second-order ones as shown in Fig. 7. This may well be an important ingredient to achieve a larger momentum aperture in the ring. It is worth noting that the choice of the beamline linear chromaticity also controls the second-order W functions.

V. CHROMATIC COMPENSATION IN A PERIODIC SYSTEM

Now, we investigate the most critical region from the IP6 to the neighboring IP8, where twice chromaticities are generated in two halves of the IRs. Naturally, we first consider the semilocal schemes outlined in the previous section. Here, we use two identical trombones on each side of the arc and four families of sextupoles to match the first-order chromatic optics. Again, the solutions are parameterized by the two linear chromaticities for the optimization of the dynamic aperture in the ring. After having corrected the chromaticity of the beamline upstream of IP6 and downstream of IP8, the achieved maximum momentum is 0.8%, slightly short of reaching our goal of 1%. The shortage is due to the steep dependence on the betatron tunes on momentum similar to the ones shown in the right side plot of Fig. 4.

In order to reach the goal, it is necessary to better control the higher order chromatic aberrations. We double the number of the variables by splitting the sextupole families at the middle of arc 7 (between IR6 and IR8) and using two trombones independently. Another reason for such a choice is to accommodate the asymmetry in the upstream and downstream of the IRs.

Since the beta functions at the IPs are identical and alpha functions are zero, it is convenient to optimize chromatic optics of this beamline as a periodical system. The 12 variables allow us to minimize up to the third-order chromaticities and chromatic beatings, characterized by 12 quantities in the first column of Table III. Their best values are tabulated in the third column in comparison to the case of the conventional two-family scheme. The improvement is dramatic, especially for the third order. The solutions are obtained by scanning the targeted linear chromaticity from −20 to 0 in both planes in this beamline. We choose the best one targeted at the value −13.

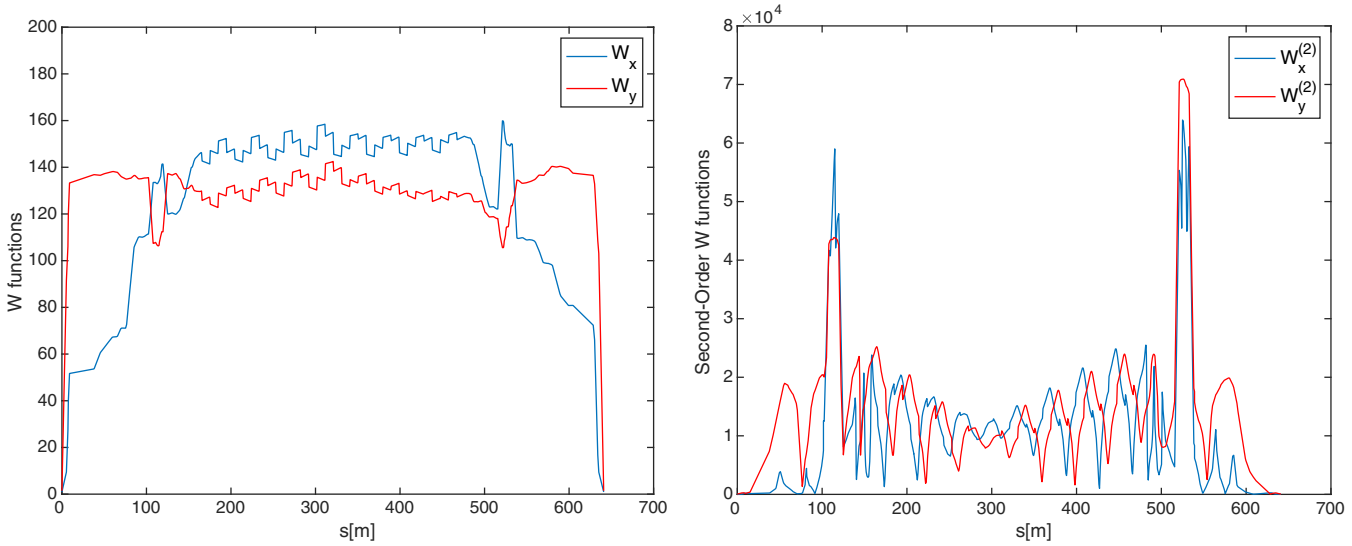

FIG. 8. Amplitudes of the first- (left) and the second-order (right) Montague functions from IR6 to IR8 using eight families of compensation sextupoles.

The initial condition in the optimization is the semilocal solution with the same linear chromaticity. The first and second order W functions are plotted in Fig. 8. The two spikes in $W^{(2)}_{x,y}$ are generated by the spin rotator quadrupoles between two solenoids, where the horizontal and vertical planes are coupled.

VI. CHROMATIC MATCHING OF THE RING

So far, we have matched the first-order chromatic optics in the first half of the ring where the two IPs are located. To match the second half, we again group the sextupoles in the remaining three arcs, namely arc-11, 1, and 3, into four families and use the trombone in the middle of the straight 12. Moreover, we insert another trombone at the center of the straight 2 to minimize the amplitudes of the W functions in the entire half of the ring. Again, the solution can be parameterized in terms of the two linear chromaticities for given phase settings of the trombones. But they are not free parameters anymore and are instead determined by the required linear chromaticities in the entire ring. In this paper, we always set the linear chromaticity to one unit in both planes.

Globally, we use two more trombones with equal phase advances at the boundaries of the two halves of the ring to retain the design tunes. Since the W functions in each half of the ring are matched to zero at the boundaries, the two halves are matched to each other. The matched solution of the entire ring is shown in the left plot of Fig. 9. However, the second-order dispersion (the first derivative in δ) in the

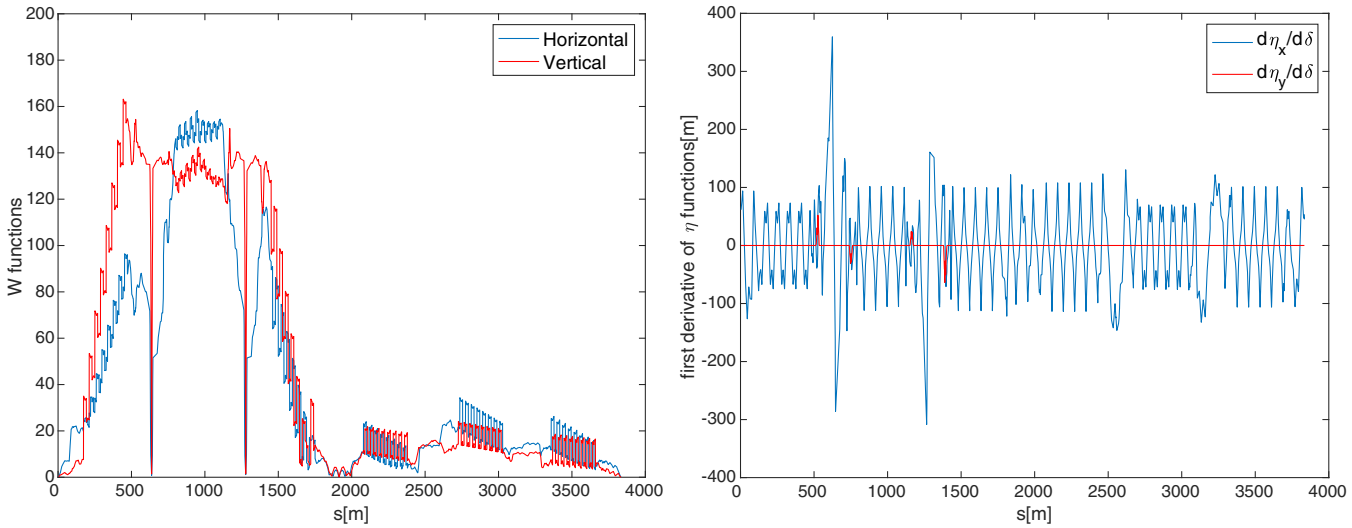

FIG. 9. The first-order chromatic optics in the electron storage ring without correction of the second-order dispersion.

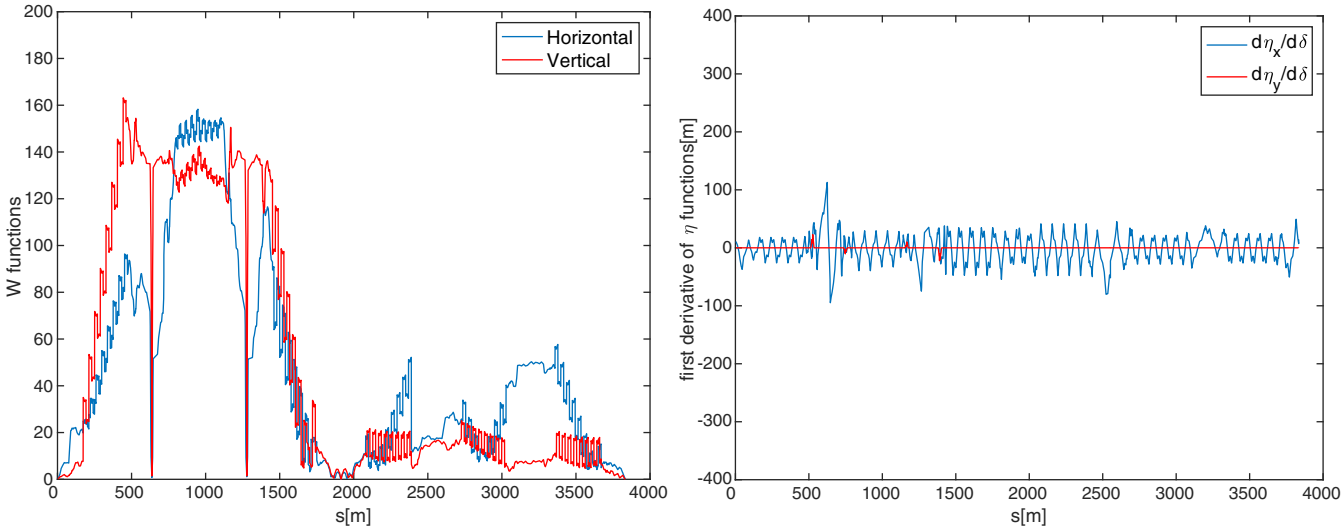

FIG. 10. The first-order chromatic optics in the electron storage ring with correction of the second-order dispersion.

horizontal plane, as depicted in the right plot, is too large. It is in the order of a meter for an off-momentum particle with 1% deviation, resulting in strong synchro-betatron resonances [21].

So where is the second-order dispersion generated? Every sextupole in the regular arcs shown in Fig. 5 is paired with another one via -I transformation. As a result, they cannot be the sources. In fact, the main sources are the bending magnets in the two IRs, where the conditions of geometry, linear optics, and spin rotation all have to be satisfied.

Fortunately, the second-order dispersion can be significantly reduced by two additional F sextupoles in the irregular cells at the edge of the arcs 3 and 11, as shown in the right plot of Fig. 10. Since the two sextupoles also change the W functions, the second half of the ring has to be rematched. The optimal solution is shown in the left plot of Fig. 10. The larger amplitudes of the W functions are a trade-off with better correction of the second-order dispersion.

VII. DYNAMIC APERTURE

The first-order chromatic matching and the correction of the second-order dispersion allow us to increase the off-momentum dynamic aperture to 1%. However, the two newly added sextupoles are so strong ($K_2 = 1,\ 5\ \mathrm{m}^{-3}$) that they severely degrade the on-momentum aperture. To understand the degradation, we compute the accumulated driving terms of the third-order resonances using the symplectic transfer map and the Lie factor f_3 [22] and then use harmonic sextupoles to correct the resonance driving terms.

The results are depicted in Fig. 11. There are no net driving terms in the first half of the ring, where all chromatic sextupoles are paired. One can clearly see huge step rises at the end of the fourth arc (arc 11), where the strongest F sextupole correcting the second-order dispersion is resided. In order to reduce these large driving terms, we use 12 harmonic sextupoles located in the straight 2, where the horizontal dispersion is zero. They are used to perform resonance driving terms correction which restores the on-momentum aperture.

The strengths of the 12 harmonic sextupoles are displayed in red color in Fig. 12 along with all other sextupoles. The length of all sextupoles is $L_S = 0.7$ m. The settings are obtained using the simplex optimizer [18] to zero out all five driving terms given in Fig 11. We find that instead of 100% cancelation of the driving terms, the solution with 75% cancelation is optimal for the dynamic

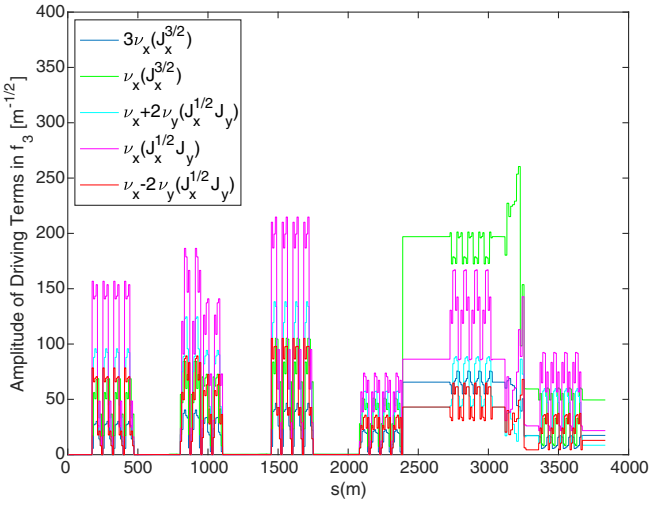

FIG. 11. The driving terms of the third-order resonances with correction by the harmonic sextupoles in the dispersion-free straight.

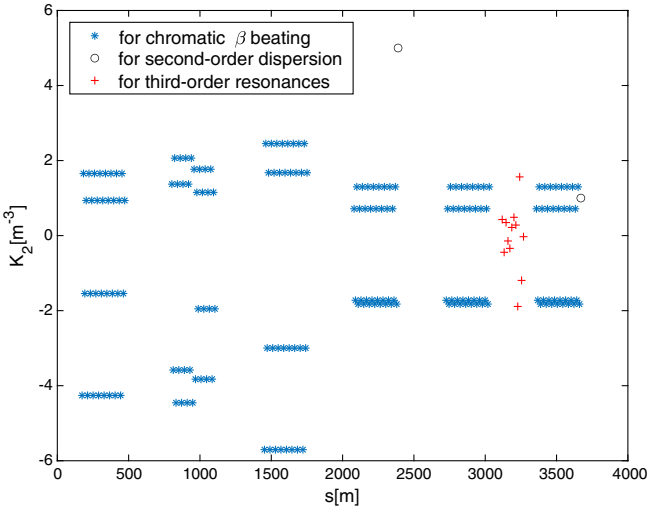

FIG. 12. Settings of all chromatic sextupoles (blue color) in the arcs and harmonic sextupoles (red color) in the dispersion-free straight.

aperture as shown in the left plot of Fig. 13 along with the chromatic tunes on the right.

As we have shown in Sec. IV, the solutions of the first-order chromatic matching can be linearly parameterized by their local linear chromaticities. Here, there are two constraints on the linear chromaticity of the ring. So, we vary four independent parameters to optimize the dynamic aperture by tracking. A simple manual search yields the best result shown in the left plot of Fig. 13. With this compensation scheme, we increase the momentum aperture from 0.5% (see Fig. 4) to 1% while retaining the good on-momentum aperture. The 1% momentum bandwidth is confirmed also by the direct calculation of the chromatic tunes in the right plot. The steep tune dependence on the momentum is removed.

VIII. PHASE TROMBONE

In our study, the phase trombone has been represented by a symplectic matrix constructed as the product of the three matrices [17]: a linear and symplectic transformation to the normalized coordinates, a rotation using the phase shifts, and the inverse transformation back to the physical coordinates.

Once an optimal solution is found, we need to implement it with actual changes of quadruples and sometimes drifts. Typically, it takes a few iterations to converge, depending on the values of the phase shifts. For implementing the trombone solution we have presented, only one iteration was required. The lattice with physical quadrupoles achieves 1.1% momentum aperture while retaining the on-momentum aperture.

IX. CONCLUSION

The optimization of the chromatic optics is essential in the design of storage rings. Historically, the computer codes, for example, HARMON [23] and SAD [24], allow us to minimize the chromatic aberrations by numerically adjusting the settings of sextupoles. This kind of optimization is useful and often adequate. Now, enormous computing power enables us to directly optimize the momentum aperture by tracking [7,25]. But the tracking method hardly provides any insights into the underlining physics, especially when it fails.

Driven by necessity, we have developed a new hybrid chromatic compensation scheme for the ESR with two neighboring IRs in the EIC. The scheme consists of the modular chromatic matching of periodic systems and beamlines. The first-order chromatic optics can be matched similarly to the linear optics: first finding a good periodic cell and then matching it to the other modules. The method

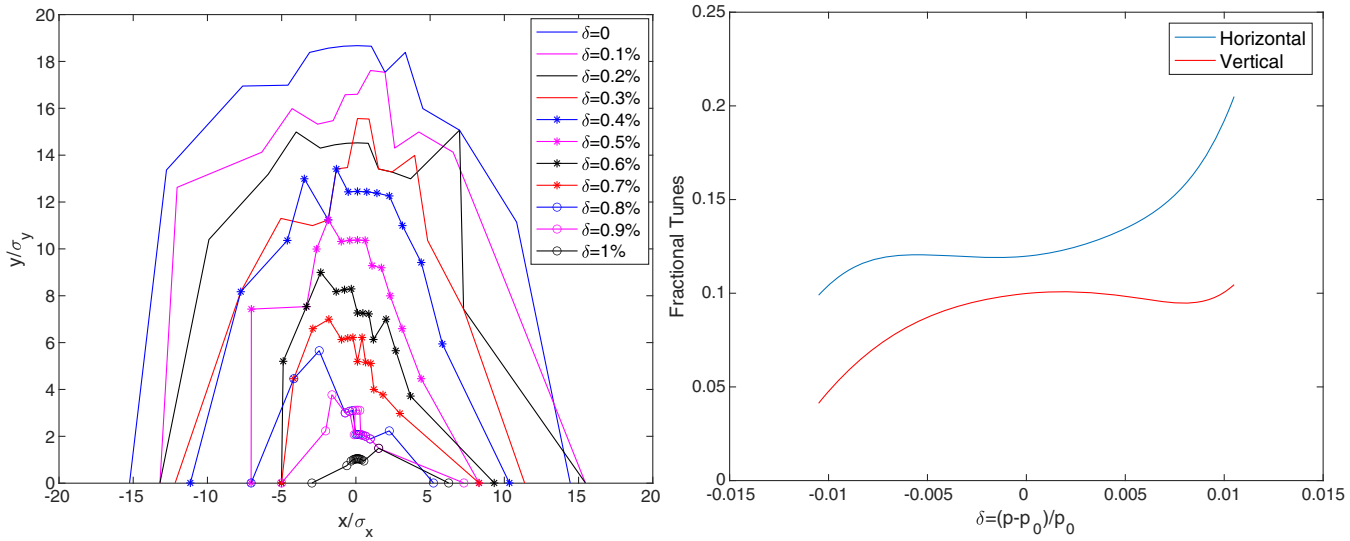

FIG. 13. Dynamic aperture (left) and chromatic tune (right) in the lattice optimized with the hybrid chromatic compensation scheme.

allows more refined and direct control of the chromatic optics, for example, achieving extremely small first-order chromatic beatings at the positions of the beam-beam collisions and rf cavities.

Moreover, we show that the first-order chromatically matched solutions are linearly parameterized with the local linear chromaticities that control the higher order chromatic beatings. The parameterization enables an efficient optimization of dynamic aperture. We find that the ring constructed by the first-order chromatically matched modules is adequate for 1% momentum aperture.

ACKNOWLEDGMENTS

This work was supported by Brookhaven Science Associates, LLC under Contract No. DE-SC001 2704 and SLAC under Contract No. DE-AC02-76SF00515 with the U.S. Department of Energy.

[1] PEP-II: An asymmetric B factory. Conceptual Design Report, Report No. SLAC-418, 1993.
[2] KEKB B-factory design Report, Report No. KEK-Report-95-7, 1995.
[3] M. Benedikt and F. Zimmermann, Outline and status for the FCC-ee Design Study, ICFA Beam Dyn. Newsl. **67**, 86 (2015).
[4] CEPC-SPPC Preliminary Conceptual Design Report, Volume **II**-Accelerator, Reports No. IHEP-CEPC-DR-2015-01, IHEP-AC-2015-01, 2015.
[5] V. I. Telnov, Restriction on the Energy and Luminosity of e^+e^- Storage Rings due to Beamstrahlung, Phys. Rev. Lett. **110**, 114801 (2013).
[6] K. L. Brown, A conceptual design of final focus systems for linear colliders, Report No. SLAC-PUB-4159, 1987.
[7] K. Oide *et al.*, Design of beam optics for the future circular collider e^+e^- collider rings, Phys. Rev. Accel. Beams **19**, 111005 (2016).
[8] S. Fartoukh, Achromatic telescopic squeezing scheme and application to the LHC and its luminosity upgrade, Phys. Rev. ST Accel. Beams **16**, 111002 (2013).
[9] E. Cruz-Alaniz, D. Newton, R. Tomas, and M. Korostelev, Design of the large hadron electron collider interaction region, Phys. Rev. Accel. Beams **18**, 111001 (2015).
[10] F. Willeke, Electron Ion Collider Conceptual Design Report 2021, Report No. BNL-221006-2021-FORE, 2021.
[11] D. Marx *et al.*, Dynamic aperture optimization in the EIC Electron Storage Ring with two interaction points, in *Proceedings of the 12th International Particle Accelerator Conference, IPAC-2021, Campinas, SP, Brazil* (JACoW Publishing, Geneva, Switzerland, 2021), TUPAB235.
[12] K. L. Brown and R. V. Servranckx, Optics modules for circular accelerator design, Nucl. Instrum. Methods Phys. Res., Sect. A **258**, 480 (1987).
[13] M. Berz, Differential algebra description of beam dynamics to very high order, Part. Accel. **24**, 109 (1989).
[14] E. Forest, M. Berz, and J. Irwin, Normal form methods for complicated periodic systems: A complete solution using differential algebra and Lie operators, Part. Accel. **24**, 91 (1989).
[15] B. W. Montague, Linear optics for improved chromaticity correction, Report No. CERN-LEP-NOTE-165, 1979.
[16] R. Brinkmann and F. Willeke, Chromatic corrections and dynamic aperture in the HERA Electron Ring II, Report No. DESY 87-037, 1987.
[17] Y. Cai, Symplectic maps and chromatic optics in particle accelerators, Nucl. Instrum. Methods Phys. Res., Sect. A **797**, 172 (2015).
[18] J. A. Nelder and R. Mead, A simplex method for function minimization, Comput. J. **7**, 308 (1965).
[19] M. Sands, A beta mismatch parameter, Report No. SLAC-AP-85; W. Spence (unpublished).
[20] M. Minty and F. Zimmermann, *Measurement and Control of Charged Particle Beams* (Springer, New York, 2003).
[21] F. Willeke, Overcoming performance limitations due to synchro-betatron resonances in the HERA Electron Ring, in *Proceedings of the 9th European Particle Accelerator Conference, Lucerne, Switzerland, 2004* (EPS-AG, Lucerne, 2004), p. 650, http://accelconf.web.cern.ch/AccelConf/e04/.
[22] Y. Cai, Single-particle dynamics in electron storage rings with extremely low emittance, Nucl. Instrum. Methods Phys. Res., Sect. A **645**, 168 (2011).
[23] M. Donald and D. Schofield, A user's guide to the HARMON program, Report No. LEP-Note-420, CERN, 1982.
[24] K. Oide, Strategic Accelerator Design, see SAD/Tkinker, KEK, http://acc-physics.kek.jp/SAD/sad.html (1997).
[25] M. Borland *et al.*, Multi-objective direct optimization of dynamic acceptance and lifetime for potential upgrades of the advanced photon light source, Argonne National Laboratory, Report No. ANL/APS/LS-319, 2010.